IMPACT OF SYNCHRONIZATION METHODS ON THE PERFORMANCE OF SELF-EXCITED INDUCTION GENERATORS

C. Rech, R. F. de Camargo, M. de Campos, F. Salvadori, G. V. Leandro, J. C. O. Bolacell
Universidade Regional do Noroeste do Estado do Rio Grande do Sul - UNIJUÍ
CEP: 98700-000 – Ijuí, RS – Brazil
cassiano@ieee.org, robinson.camargo@unijui.edu.br

***Abstract* – This paper analyzes digital sensorless control systems used to regulate the output voltages of a self-excited squirrel-cage induction generator. Different mechanical sensorless synchronization methods are evaluated and their performances are compared under several load conditions, including unbalanced and nonlinear loads. Simulation and experimental results are included to demonstrate the impact of distinct digital control systems on the output voltages distortion and the unbalance factor.**

***Keywords* – Induction generator, synchronization method, voltage control.**

I. INTRODUCTION

It is well-known that an induction machine can generate power when the rotor speed is greater than the speed of the stator rotating magnetic field, and when it is connected to an external reactive power source. In stand-alone systems, the reactive power to create the stator magnetic field can be supplied by a capacitor bank [1]. A squirrel-cage induction machine is attractive for small and medium power generation systems due to its low cost, robustness, self-protection capacity and high power density (W/kg). On the other hand, the amplitude and the frequency of the output voltages of a self-excited induction generator (SEIG) depend on the load.

Several solutions have been presented to regulate the output voltages of induction generators in stand-alone systems. Among these alternatives, it is usual to employ a pulsewidth modulated voltage-source inverter (PWM-VSI) connected in parallel with the induction generator and the ac loads [2]-[7]. The PWM-VSI operates as a static reactive power compensator, which absorbs or injects reactive power to the system according to the load to regulate the ac bus voltages.

Distinct control techniques have been developed to control the shunt connected PWM-VSI and, consequently, to regulate the output voltages under different load conditions [3]-[7]. Digital control systems without any mechanical sensor are particularly interesting, because the cost of a mechanical sensor is significant when compared to the cost of a squirrel-cage induction machine for small and medium power generation systems [7]. In addition, control systems are usually implemented in *dq* reference frame for three-phase electrical machines applications, since the tracking problem is changed to a regulation problem, making possible to use well-known proportional-integral (PI) controllers to regulate the control variables. To convert the variables from *abc* stationary reference frame to *dq* synchronous reference frame, it is necessary to use a synchronization method to compute the synchronization signals employed in the transformation. Nevertheless, the impact of distinct synchronization methods on the voltages generated by a stand-alone generation system based on a self-excited induction generator has not yet been presented.

To fill this gap, this paper analyzes digital sensorless control systems used to regulate the output voltages of a self-excited squirrel-cage induction generator. Distinct open-loop synchronization methods are evaluated and their performances are compared under several load conditions, including unbalanced and nonlinear loads. Simulation and experimental results are included to demonstrate the impact of distinct synchronization methods on the unbalance and distortion of the output voltages.

II. DESCRIPTION OF THE GENERATION SYSTEM

A simplified diagram of the system under study is shown in Fig. 1. It is composed of a squirrel-cage induction generator excited by a three-phase capacitor bank and a pulsewidth modulated voltage-source inverter. The dc bus of the inverter is composed of electrolytic capacitors as the dc voltage source. The induction generator is connected to the PWM inverter ac side through filter inductances, which composes a second-order filter with the capacitor bank to minimize high-order harmonic frequencies generated by the VSI.

The PWM-VSI should inject or absorb a reactive power level to regulate the induction generator output voltages, independent on the ac load power. The PWM-VSI acts as a capacitor and it injects reactive power in the system when the induction generator output voltages are smaller than the reference voltage. On the other hand, the PWM-VSI absorbs reactive power from the generation system when the ac bus voltages are higher than the desired value.

The sensorless digital control system employed in this paper uses the *dq* synchronous reference frame, and, therefore, the feedback variables in *abc* axis must be transformed to the *dq* axis, using the following transformation:

$$\mathbf{T}_{dq}=\begin{bmatrix} \frac{\sqrt{6}}{3}\cos(\theta) & -\frac{\sqrt{6}}{6}\cos(\theta)+\frac{\sqrt{2}}{2}\sin(\theta) & -\frac{\sqrt{6}}{6}\cos(\theta)-\frac{\sqrt{2}}{2}\sin(\theta) \\ -\frac{\sqrt{6}}{3}\sin(\theta) & \frac{\sqrt{6}}{6}\sin(\theta)+\frac{\sqrt{2}}{2}\cos(\theta) & \frac{\sqrt{6}}{6}\sin(\theta)-\frac{\sqrt{2}}{2}\cos(\theta) \end{bmatrix} \quad (1)$$

According to (1), a synchronization method should be utilized to obtain the synchronization angle θ or the sine and cosine signals used in *abc* to *dq* transformation.

Fig. 2 presents a simplified block diagram of the PWM-VSI control system. The error between the dc bus voltage and its reference value is the input of a PI controller, which generates the *d*-axis reference current (i_d^*). The *d*-axis inverter current (i_d) controls the active power flow through

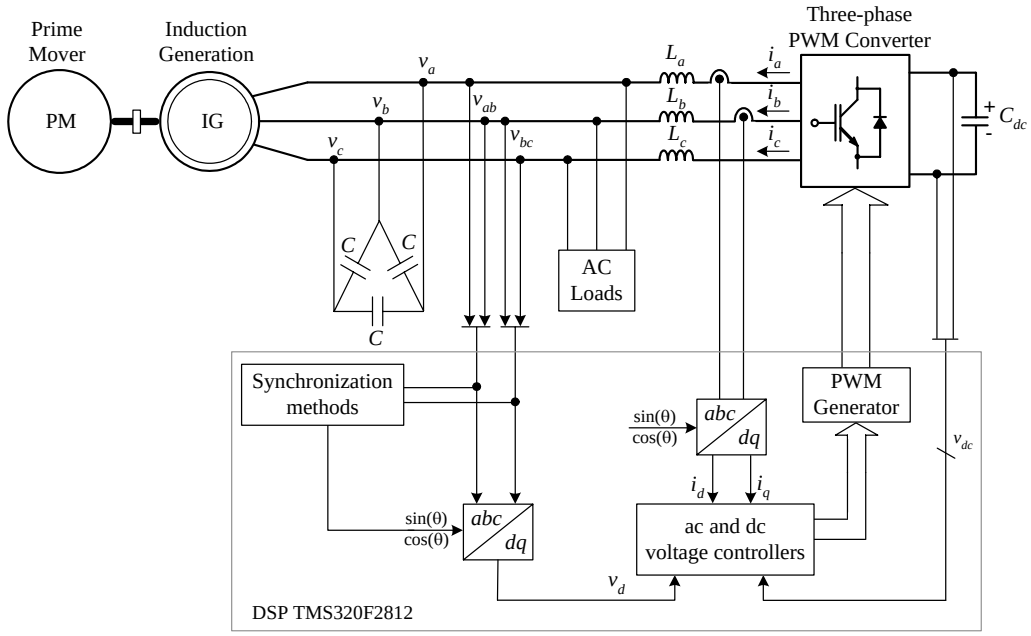

Fig. 1. Simplified diagram of the generation system.

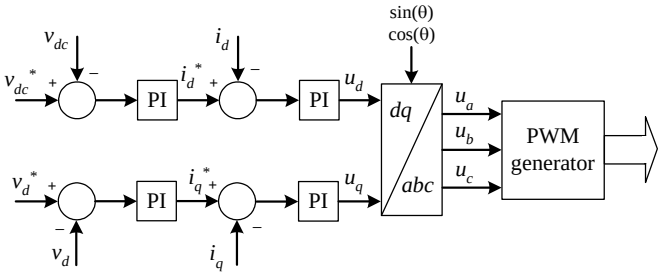

Fig. 2. Block diagram of the ac and dc voltage controllers.

the PWM inverter and, therefore, this control loop directly affects the dc bus voltage level. Similarly, the error between the induction generator output voltage in the *d*-axis and its reference value is the input of another PI controller, generating the *q*-axis reference current (i_q^*). The *q*-axis inverter current (i_q) controls the reactive power flow through the PWM-VSI, affecting the amplitude of the ac voltages generated by the system. The errors between the reference currents obtained from the outer loop voltage controllers and the measured currents are the inputs of PI current controllers, which generate the control actions in the *dq* axis.

This paper is focused on the analysis of synchronization methods used in the *abc* to *dq* transformation and vice-versa. Therefore, as the same controllers are employed for all synchronization methods presented hereinafter, the analysis and design of the controllers in not presented in this paper.

III. SYNCHRONIZATION METHODS

Synchronization techniques can be classified as closed-loop [8]-[11] or open-loop [12]-[15] methods. In the closed-loop methods the synchronization angle is obtained through a closed-loop structure, to lock the estimated value of the phase angle to its actual value. On the other hand, open-loop synchronization methods are simple, since they do not use mechanical sensors or position/speed estimation methods. The synchronization angle or the normalized synchronization vector is obtained directly from the ac voltages [12], [13] or estimated ac voltages [14]. This paper analyzes four open-loop synchronization methods that employ only two line voltages at the induction generator terminals.

A. Method I

For three-phase three-wire systems, a synchronization vector can be obtained from the measurement of only two ac line voltages [12]. Usually, PWM converters are analyzed and controlled considering phase quantities [15], then the line voltages vector, $\mathbf{v}_{ll}$, is transformed into a phase voltages vector, $\mathbf{v}_{ph}$, as illustrated in Fig. 3. Considering that the sum of the phase voltages is zero for three-wire systems, then:

$$\mathbf{v}_{ph} = \mathbf{T}_{ll-ph}\mathbf{v}_{ll} \tag{2}$$

where:

$$\mathbf{v}_{ph} = \begin{bmatrix} v_a \\ v_b \\ v_c \end{bmatrix},\ \mathbf{T}_{ll-ph} = \frac{1}{3}\begin{bmatrix} 2 & 1 \\ -1 & 1 \\ -1 & -2 \end{bmatrix},\ \mathbf{v}_{ll} = \begin{bmatrix} v_{ab} \\ v_{bc} \end{bmatrix}. \tag{3}$$

Moreover, the phase voltages are transformed into αβ coordinates, that is,

$$\mathbf{v}_{\alpha\beta} = \mathbf{T}_{\alpha\beta}\mathbf{v}_{ph} \tag{4}$$

where:

$$\mathbf{v}_{\alpha\beta} = \begin{bmatrix} v_\alpha \\ v_\beta \end{bmatrix};\ \mathbf{T}_{\alpha\beta} = \sqrt{\frac{2}{3}}\begin{bmatrix} 1 & -1/2 & -1/2 \\ 0 & \sqrt{3}/2 & -\sqrt{3}/2 \end{bmatrix}. \tag{5}$$

A normalized synchronization vector can be obtained dividing $\mathbf{v}_{\alpha\beta}$ by its norm, that is:

$$\mathbf{v}_{\alpha\beta n} = \frac{\mathbf{v}_{\alpha\beta}}{\left\|\mathbf{v}_{\alpha\beta}\right\|_2} \tag{6}$$

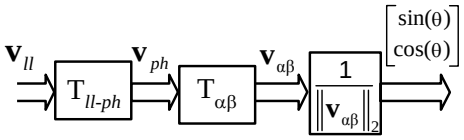

Fig. 3. Block diagram of the synchronization method I.

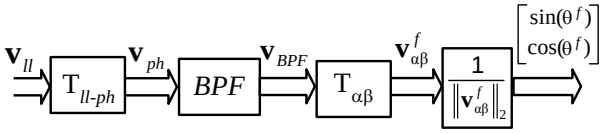

Fig. 4. Block diagram of the synchronization method II.

where the Euclidian norm of the vector is given by:

$$\left\|\mathbf{v}_{\alpha\beta}\right\|_2 = \sqrt{\left(v_\alpha\right)^2 + \left(v_\beta\right)^2}\,. \tag{7}$$

The two components of the vector $\mathbf{v}_{\alpha\beta n}$, obtained from (6), can be the cosine and sine signals used to synchronize the PWM inverter with the voltage at the generator terminals:

$$\cos(\theta) = v_{\alpha n} \quad \text{and} \quad \sin(\theta) = v_{\beta n}\,. \tag{8}$$

B. Method II

Output voltages of a SEIG can present harmonics, which can distort the synchronization signals [8] and, consequently, the voltages produced by the generation system. In order to avoid this distortion, the phase voltages vector ($\mathbf{v}_{ph}$) is filtered by band-pass filters (BPF) tuned at the fundamental frequency, as shown in Fig. 4. Ideally, the band-pass filters should have unity gain and cannot include phase-shift in the filtered signals at the fundamental frequency.

The filtered phase voltages vector ($\mathbf{v}_{BPF}$) is transformed into filtered αβ voltages ($\mathbf{v}^{\,f}_{\alpha\beta}$), by using (4) and (5). A normalized synchronization vector $\mathbf{v}^f_{\alpha\beta n}$ is obtained dividing $\mathbf{v}^{\,f}_{\alpha\beta}$ by its Euclidian norm (7). The components of the vector $\mathbf{v}^f_{\alpha\beta n}$ are the cosine and sine signals to synchronize the PWM inverter. Due to the filtering action of the band-pass filters, the normalized synchronization signals contain only the fundamental frequency.

C. Method III

Unbalanced loads can produce unbalanced voltages at the induction generator terminals. These unbalanced voltages can distort the synchronization signals and, therefore, they can affect the performance of the digital control system.

In order to avoid the harmful impact of unbalanced voltages on the synchronization signals, the synchronization vector $\mathbf{v}_{\alpha\beta+}$ is lined up with the positive sequence voltage vector. This can be carried out by using all-pass filters (APF) and $\mathbf{M}_1$ and $\mathbf{M}_2$ matrices, as shown in Fig. 5 [8], [9]. The all-pass filters are designed to result in a unity gain and 90° phase-shift at the fundamental frequency. Then, according to Fig. 5, the vector $\mathbf{v}_{\alpha\beta+}$ is computed by:

$$\mathbf{v}_{\alpha\beta+} = \mathbf{M}_2\mathbf{v}_{ph} + \mathbf{M}_1\mathbf{v}_{fil\_ph} \tag{9}$$

where matrices $\mathbf{M}_1$ and $\mathbf{M}_2$ are:

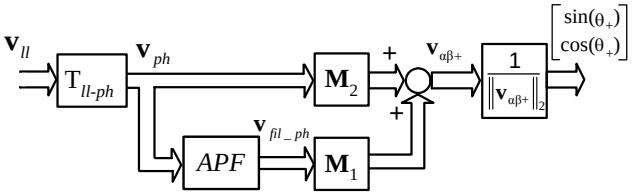

Fig. 5. Block diagram of the synchronization method III.

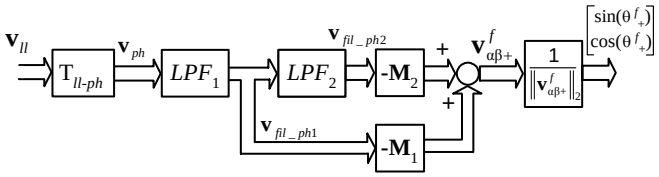

Fig. 6. Block diagram of the synchronization method IV.

$$\mathbf{M}_1 = \begin{bmatrix} 0 & \sqrt{2}/4 & -\sqrt{2}/4 \\ -\sqrt{6}/6 & \sqrt{6}/12 & \sqrt{6}/12 \end{bmatrix}$$
$$\mathbf{M}_2 = \begin{bmatrix} \sqrt{6}/6 & -\sqrt{6}/12 & -\sqrt{6}/12 \\ 0 & \sqrt{2}/4 & -\sqrt{2}/4 \end{bmatrix}. \tag{10}$$

A normalized synchronization vector $\mathbf{v}_{\alpha\beta+n}$ can be obtained dividing $\mathbf{v}_{\alpha\beta+}$, obtained from (9), by its Euclidian norm (7). Again, the components of the vector $\mathbf{v}_{\alpha\beta+n}$ are the cosine and sine signals to synchronize the PWM inverter.

It is important to highlight that the synchronization signals are computed from the positive sequence voltages and, therefore, the negative sequence voltages produced by the unbalanced loads do not affect the synchronization signals.

D. Method IV

Another synchronization method, called hereinafter of method IV, can be used to obtain low-THD synchronization signals, even with harmonic distortions and unbalanced loads [15]. In the synchronization method IV, illustrated in Fig. 6, the phase voltages vector is filtered by low-pass filters (LPF_1 and LPF_2), and the synchronization vector ($\mathbf{v}^{\,f}_{\alpha\beta+}$) is lined up with the positive sequence vector of the filtered phase voltages. So, using Fig. 6, the synchronization vector $\mathbf{v}^{\,f}_{\alpha\beta+}$ can be expressed as:

$$\mathbf{v}^f_{\alpha\beta+} = -\mathbf{M}_2\mathbf{v}^f_{fil\_ph2} - \mathbf{M}_1\mathbf{v}^f_{fil\_ph1}\,. \tag{11}$$

A normalized synchronization vector can be obtained dividing $\mathbf{v}^{\,f}_{\alpha\beta+}$ by its Euclidian norm (7). The components of the normalized synchronization vector are the cosine and sine signals to synchronize the PWM-VSI.

Similarly to the method III, the synchronization signals are obtained from the positive sequence vector of the filtered phase voltages and, consequently, the negative sequence voltages caused by unbalanced loads and harmonic distortions produced by nonlinear loads will not increase the THD of the sine and cosine signals.

IV. SIMULATION RESULTS

The generation system shown in Fig. 1 has been simulated with SimPower Systems toolbox of the Matlab/Simulink®. Table I presents the main parameters of the induction machine utilized to obtain the simulation results.

The magnetizing reactance is not constant and it depends on the magnetizing current. The relationship between the magnetizing reactance X_M and the magnetizing current I_M was obtained experimentally and is expressed as:

$$X_M(I_M) = -0.0099 I_M^4 + 0.274 I_M^3 - 2.713 I_M^2 + 9.357 I_M + 15.821 \quad (12)$$

Firstly, the synchronization method I was used to verify the performance of the generation system under sudden load changes. Fig. 7 presents the line voltage waveforms at the induction generator terminals (top) and the respective normalized *d*-axis voltage waveform (bottom) for a step load change from no-load to a balanced three-phase 3 kW resistive load. One can see that the closed-loop control system regulates the generator voltage even under this large load change.

Other load conditions were also simulated. For instance, Fig. 8 shows the synchronization signal waveforms (top) and the line voltages at the induction generator terminals (bottom) when a single-phase 1 kW resistive load is connected between two terminals of the induction generator. One can verify that the synchronization signals and the generator voltages (THD = 3.42%) present significant distortions by using the synchronization method I.

TABLE I – PARAMETERS OF THE INDUCTION GENERATOR.

Rated power	5 cv
Rated voltage	220 V (Δ connected)
Rated speed	1730 RPM
Rated frequency	60 Hz
Stator resistance	0.44 Ω
Rotor resistance	0.43 Ω
Leakage stator reactance	0.83 Ω
Leakage rotor reactance	0.83 Ω
Iron and mechanical losses resistance	232.3 Ω
Rotor inertia	0.03 kg.m^2

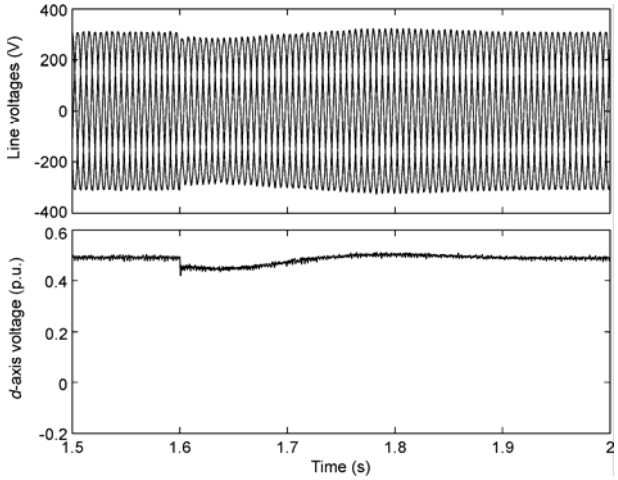

Fig. 7. Transient performance of the generation system using the synchronization method I: line voltages at the induction generator terminals (top) and *d*-axis voltage (bottom).

Nevertheless, the synchronization method III uses only the positive sequence of the induction generator voltages and, therefore, the synchronization signals will not be distorted. Fig. 9 illustrates a simulation result for the same unbalanced load used in the previous simulation, but now using the method III. It can be seen that the synchronization signals present a smaller distortion than by using the method I, and the THD of the generator voltages was reduced to 1.53%.

Several other simulations were carried out for distinct load conditions and their results are given in Tables II, III and IV.

Table II clearly shows that the synchronization signals generated by method I present a significant THD for nonlinear or unbalanced loads. On the other hand, it is possible to reduce the THD of the synchronization signals for nonlinear loads by using the methods II or IV. For unbalanced loads, it is possible to reduce the distortion of the synchronization signals by using the methods III or IV.

The generation of low-distortion synchronization signals reflects in generator voltages with smaller THDs, as can be seen in Table III. The THD of the line voltages produced by the generation system with single-phase loads is considerably

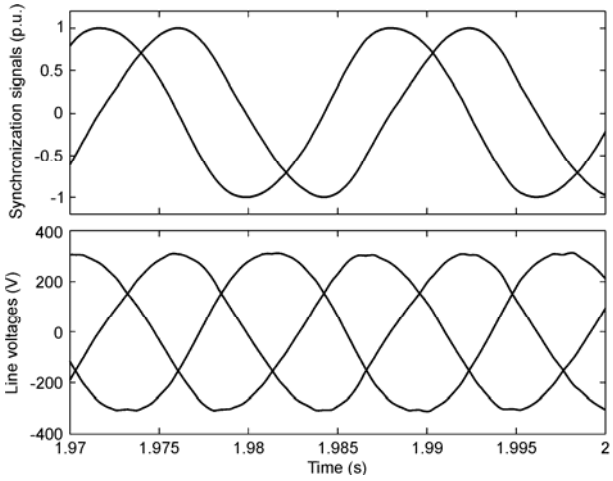

Fig. 8. Steady-state performance of the generation system using the synchronization method I under an unbalanced load: synchronization signals (top) and line voltages at the induction generator terminals (bottom).

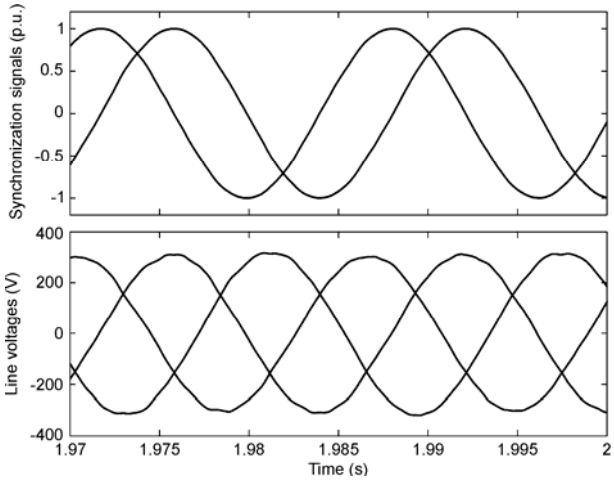

Fig. 9. Steady-state performance of the generation system using the synchronization method III under an unbalanced load: synchronization signals (top) and line voltages at the induction generator terminals (bottom).

TABLE II – THD OF THE SYNCHRONIZATION SIGNALS.

	Method I		Method II		Method III		Method IV	
	sin	cos	sin	cos	sin	cos	sin	cos
No-load	1.26	1.1	0.15	0.16	0.82	0.79	0.05	0.06
3Φ resistive load (3000 W)	1.1	0.98	0.18	0.19	0.62	0.55	0.15	0.15
Nonlinear load	5.17	5.05	0.7	0.7	3.49	3.54	0.09	0.09
1Φresistive load (1000 W)	3.7	3.57	1.9	1.91	0.84	0.75	0.05	0.07

TABLE III – THD OF THE LINE VOLTAGES AT THE GENERATOR TERMINALS.

	Method I	Method II	Method III	Method IV
No-load	1.47	1.14	1.45	1.24
3Φ resistive load (3000 W)	1.26	0.88	1.13	0.93
Nonlinear load	7.11	5.75	8.58	6.05
1Φ resistive load (1000 W)	3.42	2.12	1.53	1.19

TABLE IV – UNBALANCE FACTOR OF THE LINE VOLTAGES AT THE GENERATOR TERMINALS.

	Method I	Method II	Method III	Method IV
No-load	0.23	0.05	0.06	0.05
3Φ resistive load (3000 W)	0.01	0.06	0.04	0.04
Nonlinear load	0.06	0.02	0.08	0.04
1Φ resistive load (1000 W)	3.88	3.43	2.34	2.29

reduced by using the methods III or IV. On the other hand, for nonlinear loads, the generator voltages are less distorted by using the method II, although this reduction is not too significant. An important THD reduction for nonlinear loads can be achieved by using method II and IV, and replacing the PI current controllers by repetitive controllers, which minimize tracking errors for periodic disturbances [16].

Table IV shows that the unbalance factor of the line voltages by applying a single-phase load at the induction generator terminals is reduced by using the synchronization method IV instead of method I.

V. EXPERIMENTAL RESULTS

A prototype was built in our lab to carry out the experimental tests in the generation system presented in Fig. 1. The parameters of the induction generator are the same utilized to obtain the simulation results. The digital control system was implemented with the DSP TMS320F2812 from Texas Instruments.

Fig. 10 presents the line voltage waveforms at the stand-alone induction generator terminals before connecting the PWM-VSI to regulate the output voltages. One can observe that the voltage waveforms produced by the generator are distorted (THD = 2.1%) and this will affect those synchronization methods that are sensitive to harmonics. This effect can be verified in Fig. 11, which presents the line voltage waveforms at the induction generator terminals by employing the method I. Fig. 11(a) shows the line voltages (THD = 3.2%) by connecting a balanced three-phase 3 kW resistive load. Fig. 11(b) presents the line voltage waveforms (THD = 4.6%) with a single-phase 1 kW resistive load, which increases the harmonic distortions at the generated voltages due to the unbalanced load.

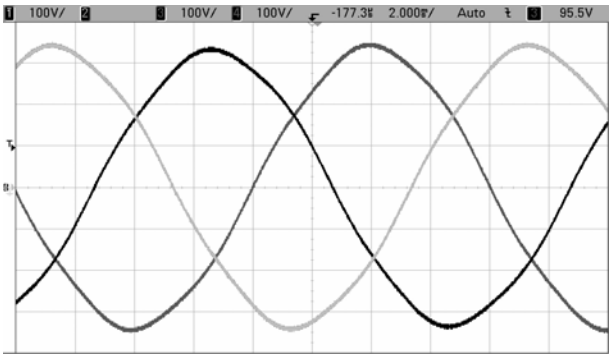

Fig. 10. Experimental result: Line voltages at the induction generator terminals before connecting the PWM-VSI.

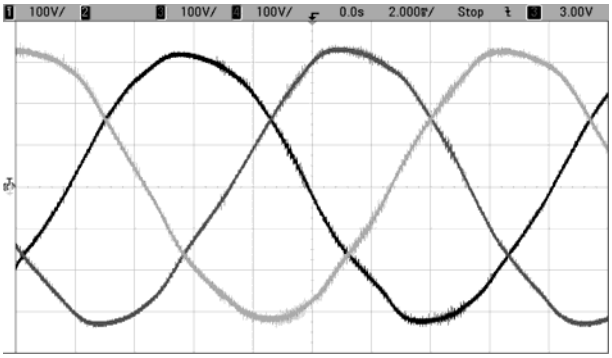

(a)

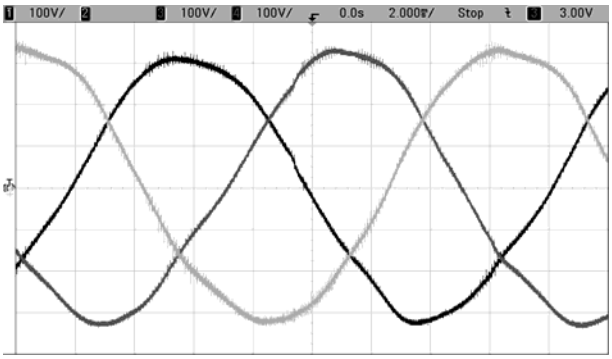

(b)

Fig. 11. Experimental result: Line voltages at the induction generator terminals using the synchronization method I. (a) Balanced three-phase 3 kW resistive load. (b) Single-phase 1 kW resistive load.

On the other hand, Fig. 12 shows the steady-state performance of the generation system by using the synchronization method IV. Fig. 12(a) presents the output voltages (THD = 1.8%) with a balanced three-phase 3 kW resistive load, while Fig. 12(b) shows the line voltage waveforms (THD = 2%) with the same unbalanced load employed to obtain the results presented in Fig. 11(b). In both cases it is possible to see a significant reduction on the THD levels by using the synchronization method IV.

Finally, Fig. 13 presents the line voltage waveforms at induction generator terminals for a step load change from no-load to a balanced three-phase 3 kW resistive load. One can see the satisfactory transient performance of the closed-loop control system even under this large load change.

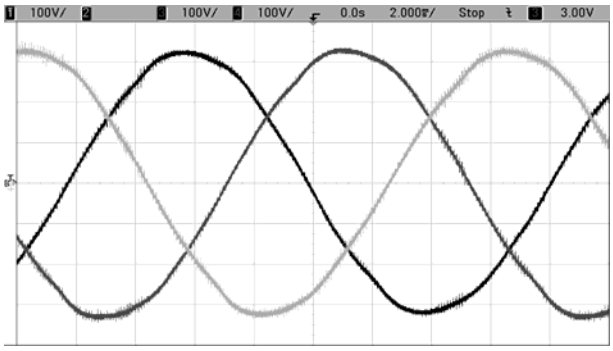

(a)

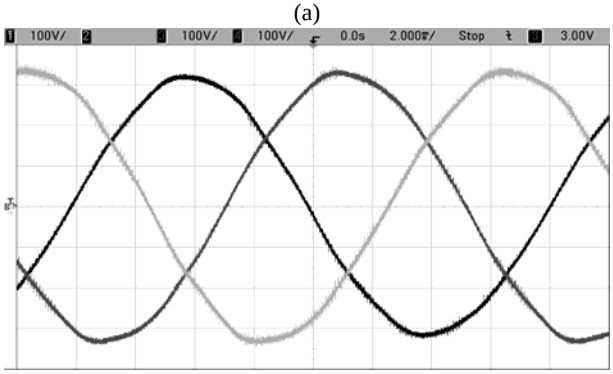

(b)

Fig. 12. Experimental result: Line voltages at the induction generator terminals using the synchronization method IV. (a) Balanced three-phase 3 kW resistive load. (b) Single-phase 1 kW resistive load.

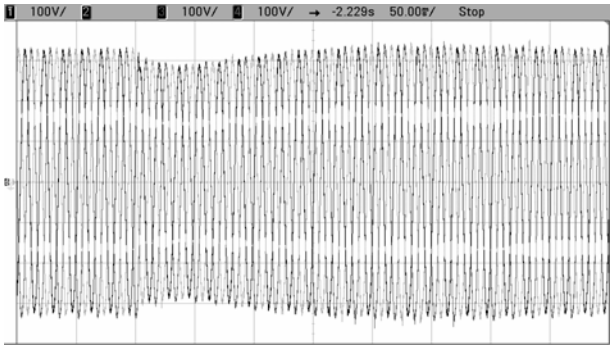

Fig. 13. Experimental result: Transient performance of the generation system using the synchronization method IV.

VI. CONCLUSION

This paper presented an evaluation of distinct open-loop synchronization methods to be applied in self-excited squirrel-cage induction generators under distinct load conditions. These synchronization methods were chosen because they present a considerable cost reduction if compared to those methods that use position or speed sensors. Results show that the impact of these methods on the THD and the unbalance factor of ac voltages produced by the generation system is significant.

The synchronization methods presented in this paper differ in terms of complexity and performance. Method I is very simple, resulting in a reduced computation time, but the synchronization signals are distorted by unbalanced and nonlinear loads. Then, it is not possible to generate low-THD voltages, even using high-performance controllers. On the other hand, method IV requires a higher computation time than those spent by other methods presented here, but the synchronization signals and the output voltages have a smaller THD, even with unbalanced and nonlinear loads.

ACKNOWLEDGEMENT

The authors would like to thank DEMEI (Departamento Municipal de Energia de Ijuí) by the financial support. Our special thanks to Prof. Fernando Botterón and to Prof. Victor Hugo Kurtz from Universidad Nacional de Misiones (UNAM) for their help along this work.

REFERENCES

[1] D. E. Basset, M. F. Potter, “Capacitive excitation for induction generators”, *AIEE Trans.*, vol. 54, pp. 540-545, May 1935.

[2] B. Singh, S. S. Murphy, S. Gupta, “Analysis and design of STATCOM-based voltage regulator for self-excited induction generators”, *IEEE Trans. Energy Conv.*, vol. 19, n. 4, pp. 783-790, Dec. 2004.

[3] L. A. C. Lopes, R. G. Almeida, “Wind-driven self-excited induction generator with voltage and frequency regulated by a reduced rating voltage source inverter”, *IEEE Trans. Energy Conv.*, vol. 21, n. 2, pp. 297-304, June 2006.

[4] E. G. Marra, J. A. Pomilio, “Self-excited induction generator controlled by a VS-PWM bidirectional converter for rural applications”, *IEEE Trans. Ind. Applicat.*, vol. 35, n. 4, pp. 877-883, Jul./Aug. 1999.

[5] S.-C Kuo, L. Wang, “Analysis of voltage control for a self-excited induction generator using a current-controlled voltage source inverter (CC-VSI)”, *IEE. Proc. – Gener., Transm. Distrib.*, vol. 148, n. 5, pp. 431-438, Sept. 2001.

[6] R. Leidhold, G. Garcia, M. I. Valla, “Induction generator controller based on the instantaneous reactive power theory”, *IEEE Trans. Energy Conv.*, vol. 17, n. 3, pp. 368-373, Sept. 2002.

[7] T. Ahmed, K. Nishida, M. Nakaoka, “Advanced control of PWM converter with variable-speed induction generator”, *IEEE Trans. Ind. Applicat.*, vol. 42, n. 4, pp. 934-945, Jul./Aug. 2006.

[8] S.-J. Lee, J.-K. Kang, S.-K. Sul, “A new phase detecting method for power conversion systems considering distorted conditions in power system”, *in Proc. of IAS*, vol. 4, pp. 2167-2172, 1999.

[9] M. Karimi-Ghartemani, M. R. Iravani, “A method for synchronization of power electronic converters in polluted and variable-frequency environments”, *IEEE Trans. Power Systems*, vol. 19, no. 3, pp. 1263-1270, Aug. 2004.

[10] S. M. Deckmann, F. P. Marafão, M. S. Pádua, “Single and three-phase digital PLL structures based on instantaneous power theory”, *in Proc. of COBEP*, pp. 225-230, 2003.

[11] E. Sasso, G. Sotelo, A. Ferreira, E. Watanabe, M. Aredes, P. Barbosa, “Investigação dos modelos de circuitos de sincronismo trifásicos baseados na teoria de potências real e imaginária instantâneas (p-PLL e q-PLL)”, *in Proc. of CBA*, 2002.

[12] G. D. Marques, “A comparison of active power filter control methods in unbalanced and non-sinusoidal conditions,” *in Proc. IECON'98*, 1998, pp. 444-449.

[13] J. Svensson, “Synchronization methods for grid-connected voltage source converters,” *IEE Proc.-Gener. Transm. Distrib.*, vol. 148, no. 3, pp. 229-235, May 2001.

[14] R. Kennel, M. Linke, P. Szczupak, “Sensorless control of 4-quadrant-rectifiers for voltage source inverters (VSI)”, *in Proc. of PESC*, pp. 1057-1062, 2003.

[15] R. F de Camargo, H. Pinheiro, “Synchronization method for three-phase PWM converters under unbalanced and distorted grid”, *IEE Proc.-Electr. Power Appl.*, vol. 153, no. 5, pp.763-772, Sep. 2006.

[16] C. Rech, H. Pinheiro, H. Gründling, H. L. Hey, J. R. Pinheiro, “Comparison of digital control techniques for low cost PWM inverters”, *IEEE Trans. Power Electr.*, vol. 18, n. 1, pp. 401-410, Jan. 2003.